ISSN 1063-7834, Physics of the Solid State, 2020, Vol. 62, No. 7, pp. 1172–1178. © Pleiades Publishing, Ltd., 2020.
Russian Text © The Author(s), 2020, published in Fizika Tverdogo Tela, 2020, Vol. 62, No. 7, pp. 1043–1049.

MAGNETISM

Features of Relaxation of the Remanent Magnetization of Antiferromagnetic Nanoparticles by the Example of Ferrihydrite

D. A. Balaev[a, b, *], A. A. Krasikov[a], A. D. Balaev[a], S. V. Stolyar[a, b, c], V. P. Ladygina[b], and R. S. Iskhakov[a]

[a] *Kirensky Institute of Physics, Krasnoyarsk Scientific Center, Siberian Branch, Russian Academy of Sciences, Krasnoyarsk, 660036 Russia*

[b] *Siberian Federal University, Krasnoyarsk, 660041 Russia*

[c] *Krasnoyarsk Scientific Center, Siberian Branch, Russian Academy of Sciences, Krasnoyarsk, 660036 Russia*

**e-mail: dabalaev@iph.krasn.ru*

Received February 20, 2020; revised February 20, 2020; accepted February 20, 2020

Abstract—The relaxation of the remanent magnetization of antiferromagnetically ordered ferrihydrite nanoparticles at the exchange bias effect implemented in these systems has been investigated. The magnetization relaxation depends logarithmically on time, which is typical of the thermally activated hoppings of particle magnetic moments through the potential barriers caused by the magnetic anisotropy. The barrier energy obtained by processing of the remanent magnetization relaxation data under the field cooling conditions significantly exceeds the barrier energy under standard (zero field cooling) conditions. The observed difference points out the possibility of using the remanent magnetization relaxation to analyze the mechanisms responsible for the exchange bias effect in antiferromagnetic nanoparticles and measure the parameters of the exchange coupling of magnetic subsystems in such objects.

Keywords: antiferromagnetic nanoparticles, ferrihydrite, exchange bias, magnetization relaxation

DOI: 10.1134/S1063783420070033

1. INTRODUCTION

The magnetic properties of nanoparticles of antiferromagnetic (AFM) materials are qualitatively different from the magnetic properties of bulk antiferromagnets. This is due to the decisive role of the surface effects in particles of small sizes. In addition, bulk defects in antiferromagnet nanoparticles are important, since they lead to decompensation of spins in sublattices and induce the uncompensated magnetic moment in AFM nanoparticles [1–3]. As a result, several magnetic subsystems are formed in AFM nanoparticles, including the ferromagnetic (FM) subsystem (uncompensated moment) [4–15], surface spins [9, 14–24], and the antiferromagnetically ordered core [25]. The presence of these subsystems and their interaction give rise to a number of bright effects observed when studying the magnetic properties of AFM nanoparticles [18–22]. One of these effects is the shift of the magnetic hysteresis loop upon cooling in an external field.

This effect named the exchange bias was first detected on submicron Co/CoO particles [26] with a pronounced FM(Co)/AFM(CoO) magnetic structure. In submicron particles or, in the ideal case, thin-film FM/AFM structures, the shift of the magnetic hysteresis loop along the abscissa axis (external field) occurs upon cooling a system in an external magnetic field starting with a temperature higher than the Néel point of an antiferromagnet (the Curie point of a ferromagnet) [27–29]. The exchange coupling between a ferromagnet and an antiferromagnet at the FM/AFM interface induces the observed effect [27–29].

However, such an effect is observed quite frequently in chemically homogeneous nanoparticles of AFM materials [11, 12, 20, 30–43]. Here, a necessary condition for the implementation of the exchange bias effect is the presence of at least two magnetic subsystems. To experimentally observe the exchange bias effect in AFM nanoparticles, it is sufficient to cool a material in an external field starting with a temperature higher than the superparamagnetic (SPM) blocking temperature, which, as a rule, is lower than the Néel temperature. In addition, in AFM nanoparticles, the shift of the magnetic hysteresis loop along the ordinate axis is often observed. Note that the mechanisms responsible for the exchange bias effect in AFM nanoparticles are still unclear and the magnetic parameters the measurement of which would yield reliable information for determining the value of the exchange coupling between the magnetic subsystems are not distinguished.

Ferrihydrite with the nominal formula $Fe_2O_3 \cdot nH_2O$ is characterized by the AFM ordering and only exists in the form of nanoparticles no larger than 8 nm in size. It is included in ferritin, which plays an important role in the vital activity of living organisms. Ferrihydrite can be obtained by chemical methods [44] or extracted from products of the vital activity of microorganisms [45, 46]. In some studies [11, 12, 36–43], the shift of the magnetic hysteresis loop upon cooling the ferrihydrite samples from a temperature higher than the SPM blocking temperature was observed. However, ferrihydrite nanoparticles exhibit, as a rule, fairly high fields (about 10^5 Oe) of the irreversible magnetization behavior and a problem of separating the exchange bias effect from the effect related to minor hysteresis loops arises [40–42]. In [42], a method was proposed for identifying the exchange bias effect; it was established that, in the investigated series of ferrihydrite samples, this effect exists at a nanoparticle size of more than 3 nm.

The hysteresis of any physical quantity is related to the relaxation processes and the exchange bias effect should obviously be reflected in the magnetization relaxation. In this work, we studied the relaxation of the remanent magnetization of a ferrihydrite sample with an average particle size of 4 nm under the exchange bias (external field cooling) and standard (zero field cooling) conditions. The main aim of this study was to establish the possibility of using the magnetization relaxation data for distinguishing the parameters that characterize the exchange coupling of magnetic subsystems in the investigated antiferromagnetically ordered ferrihydrite nanoparticles.

2. EXPERIMENTAL

The biogenic ferrihydrite samples were extracted from bacterial sediments after culturing Klebsiella oxytoca bacteria under anaerobic conditions [11, 45, 46]. The obtained dried sol is an aggregated system of ferrihydrite nanoparticles coated with an organic shell [47] with a small (about 2–3 nm) average size. The systems of different series obtained in this way have identical particle sizes and their characteristic SPM blocking temperatures TB lie in a narrow range (23–25 K in fields of up to 1 kOe) [11, 13, 43]. As was shown previously [12, 13, 48], the low-temperature (up to ~200°C) annealing of ferrihydrite in air leads to a controlled increase in the size of particles in aggregated systems, while other iron oxide or hydroxide modifications are not formed upon the annealing. The sample used in this work for studying the magnetization relaxation and magnetic hysteresis loop was annealed at 200°C for 24 h. The average particle size in this system, according to the transmission electron microscopy data, was ~4 nm [42]. This aggregate is hereinafter referred to as FH-4 nm.

The magnetic measurements were performed on a vibrating sample magnetometer [49]. The investigated powder was fixed in a measuring capsule using paraffin. The temperature dependences of the magnetization ($M(T)$) were measured under the zero field cooling (ZFC) conditions and upon cooling in an external field (field cooling, FC). The magnetization hysteresis ($M(H)$ loops recorded in the ZFC mode at $T = 4.2$ K were obtained up to different maximum applied fields $\pm H_{max}$ with a gradually increasing $|H_{max}|$ value. The FC $M(H)$ dependences ($T = 4.2$ K) were measured upon cooling in fields of $H_{FC} = +30$ kOe and +45 kOe starting with a temperature of 120 K, which significantly exceeds the temperature of the irreversible behavior of the $M(T)$ dependences.

The magnetization relaxation was measured at $T =$ 4.2 K after meeting the FC conditions at $H_{FC} =$ +30 kOe and a subsequent decrease in the field to zero, as well as under the ZFC conditions after applying fields of up to 30 kOe and decreasing the field to zero. In both cases, a decrease in the remanent magnetization M_R with time (the $M_R(t)$ dependence) was detected. In these measurements, after stopping at $H = 0$ for 4500 s, the hysteresis loop was continued to be measured.

3. RESULTS AND DISCUSSION

Figure 1 shows the ZFC and FC $M(T)$ dependences for the investigated ferrihydrite nanoparticle sample in different magnetic fields. One can see the behavior typical of SPM systems, specifically, the nonmonotonic ZFC $M(T)$ dependences with a maximum at the characteristic SPM blocking temperature ($T_B \sim 60$ K at $H = 1$ kOe), the discrepancy between the ZFC and FC $M(T)$ dependences in the vicinity of the temperature T_B, and the T_B shift to the low-temperature region with increasing external field.

Figure 2 shows the $M(H)$ magnetic hysteresis loops at $T = 4.2$ K obtained in the ZFC mode in maximum applied fields of $H_{max} = \pm 30$ and ± 60 kOe and in the FC mode in a field of $H_{FC} = +30$ kOe. The FC hysteresis loop noticeably shifts both along the abscissa and ordinate axis. Figure 3 shows the portions of the FC and ZFC $M(T)$ dependences in the vicinity of the intersection with the ordinate axis in the positive M range. Here, we present the data of the measurements of two types: (i) standard loop recording in the $\pm H_{FC}$ or $\pm H_{max}$ range in the ZFC mode and (ii) loop recording with the stopping at $H = 0$ for 4500 s. The noticeable relaxation of the remanent magnetizations M_{R_FC} (the FC mode) and M_{R_ZFC} (the ZFC mode) are observed for both magnetic prehistories.

Usually, the parameter characterizing the exchange bias in the FM/AFM structures is

$$H_{EB} = -(H_{CL} + H_{CR})/2, \quad (1)$$

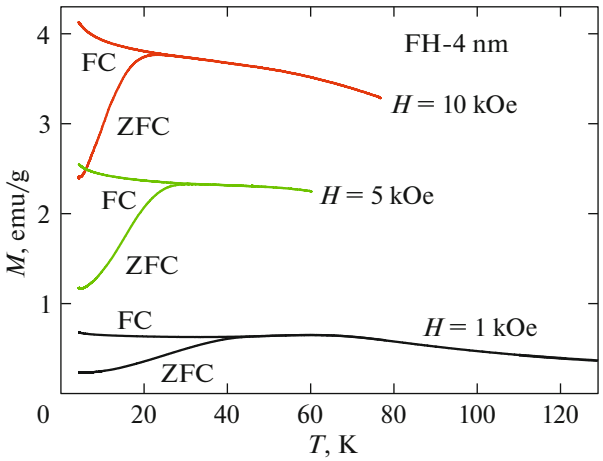

Fig. 1. ZFC and FC $M(T)$ dependences for sample FH-4 nm in different magnetic fields.

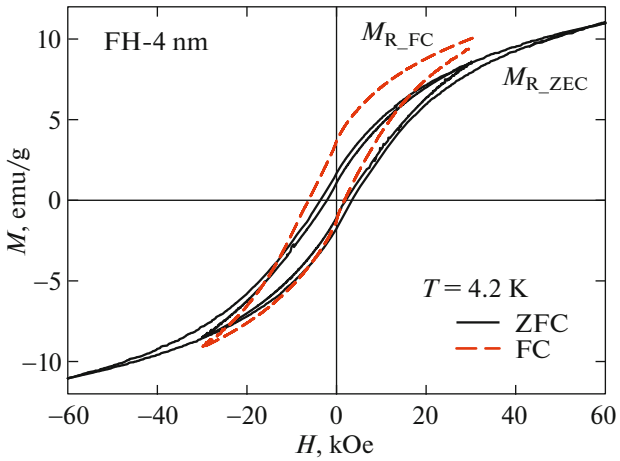

Fig. 2. $M(H)$ dependences recorded at $T = 4.2$ K under the ZFC (H_{max} = 30 and 60 kOe) and FC (H_{FC} = +30 kOe) conditions.

where H_{CL} and H_{CR} are the left and right coercivities of the hysteresis loops under the FC conditions at $H_{FC} > 0$, respectively [27–29]. Obviously, we have $H_{EB} \neq 0$ at $|H_{CL}| > |H_{CR}|$ or, equivalently, at $|H_{CL}| > |H_C|$ (hereinafter, H_C is the coercivity on the symmetrical ZFC loop). However, the hysteresis loops of sample FH-4 nm remain open under the ZFC conditions in fields of up to 60 kOe (see Fig. 2) and the H_C value of the total hysteresis loop is unknown. Then, Eq. (1) becomes inapplicable, since the shift of the loop can simply be a consequence of the minor hysteresis loop [29]. Therefore, it is necessary to determine the ZFC coercivity at the large H_{max} value by extrapolating the $H_C(H_{max})$ dependence to a certain constant H_{C_INF} value at $H_{max} \to \infty$. Then, we can compare the $|H_{CL}|$ and H_{C_INF} values and the exchange bias field is already determined by the formula [42]

$$H_{EB} = |H_{CL}| - |H_{C\_INF}|. \quad (2)$$

In principle, the $H_C(H_{max})$ dependence can be approximated by a certain function that describes the experimental H_C and H_{max} points and tends to saturation at large H_{max} values. As was shown in [41], for AFM ferrihydrite nanoparticles, the equation

$$H_C(H_{max}) = H_{C\_INF}[1 - H^*/H_{max}]^b \quad (3)$$

with an exponent of $b = 1.5$ is valid. The processing of the experimental data obtained on sample FH-4 nm yields $|H_{C\_INF}| \approx 4.75$ kOe, which corresponds to $H_{EB} \approx 1.25$ kOe at $|H_{CL}| \approx 6$ kOe.

Let us consider the shift of the FC magnetic hysteresis loop along the ordinate axis. The remanent magnetization M_{R_FC} after cooling in external field significantly exceeds the ZFC remanent magnetization M_{R_ZFC} (see Figs. 2, 3). However, the M_{R_ZFC} value, similar to the H_C value, depends on H_{max}. Above, we described the procedure for determining the H_{C_INF} value. The ZFC remanent magnetization M_{R_INF} at the large H_{max} value can also be determined by extrapolating the dependence of M_{R_ZFC} on H_{max} to a certain constant value at $H_{max} \to \infty$. The data presented in Fig. 4 illustrate the desired dependence of M_{R_ZFC} on H_{max} obtained from the minor ZFC hysteresis loops. It can be seen that this dependence also tends to saturation (plateau) at the large H_{max} values. The analysis of the data presented in Fig. 4 showed that the

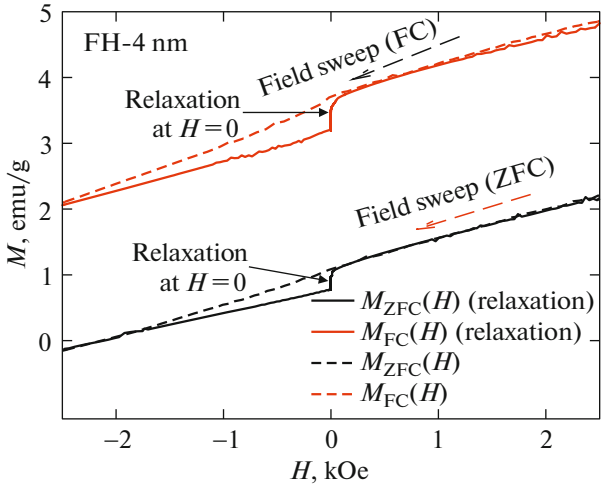

Fig. 3. Portions of the $M(H)$ dependences obtained under the FC (H_{FC} = +30 kOe) and ZFC (H_{max} = 30 kOe) conditions in a conventional way and with the stopping at $H = 0$ with the recording of the relaxation of remanent magnetization M_{R_FC} for 4500 s.

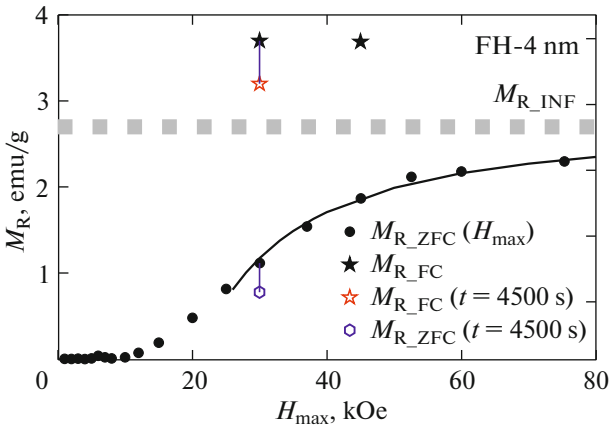

Fig. 4. Remanent magnetization M_{R_ZFC} as a function of the maximum applied field H_{max} under the ZFC conditions. Remanent magnetization M_{R_FC} under the FC conditions in fields of 30 and 45 kOe (the positions of the M_{R_FC} points on the abscissa axis correspond to these field values) and remanent magnetizations $M_{R\_FC}(t$ = 4500 s) and $M_{R\_ZFC}(t = 4500$ s) after relaxation for 4500 s (connected to the values $M_{R\_FC}(t = 0)$ and $M_{R\_ZFC}(t = 0)$ by vertical lines). The solid curve is built using Eq. (4) at $H^* = 22$ kOe, $b = 1.5$, and $M_{R\_INF} = 2.7$ emu/g. The horizontal dashed line shows the M_{R_INF} position relative to the other data.

$M_{R\_ZFC}(H_{max})$ dependence in sufficiently strong fields can be described by the function similar to (3)

$$M_{R\_ZFC}(H_{max}) = M_{R\_INF}[1 - H^*/H_{max}]^b \qquad (4)$$

with the exponent $b = 1.5 \pm 0.2$; the variation in b within these limits weakly affects M_{R_INF}. The solid curve in Fig. 4 was built using Eq. (4) at $b = 1.5$ and corresponds to the best fitting of the experimental points. The horizontal dashed line corresponds to the M_{R_INF} value in Eq. (4) and the line thickness shows the estimated M_{R_INF} error. Figure 4 shows also the remanent magnetizations of the FC $M(H)$ loops M_{R_FC} at $H_{FC} = 30$ and 45 kOe (the position of the M_{R_FC} points on the abscissa axis corresponds to the field H_{FC} in which the sample was cooled). It can be seen that the cooling field value almost does not affect the remanent magnetization ($M_{R_FC}(H_{FC} = 30$kOe) $\approx$ $M_{R\_FC}(H_{FC} = 45$ kOe)). In addition, it can be seen that the M_{R_FC} value is significantly greater than M_{R_INF}. The latter can be caused by the exchange bias effect.

To describe the exchange bias effect in the FM/AFM film structures, the specific binding energy σ_S at the FM/AFM interface is introduced. For such objects ideal in terms of the morphological parameters, the σ_S value can be obtained knowing the saturation magnetization M_S of a ferromagnet, its layer thickness d_{FM}, and exchange bias field H_{EB} [27–29, 50]

$$\sigma_S = H_{EB}M_S d_{FM}. \qquad (5)$$

For AFM nanoparticles, which are morphologically nonideal objects, the analysis using Eq. (5) can only be made under certain assumptions. First, the main contribution to the $M(H)$ hysteresis is made by the uncompensated magnetic moments of particles (the FM subsystem); therefore, the exchange coupling is implemented both between the FM subsystem and the AFM particle core and between the FM subsystem and the subsystem of surface spins. Second, the parameter d_{FM}, i.e., the FM layer thickness, is undetermined in our case; we can unambiguously indicate only the inequality $d_{FM} \le D$ (D is the particle size). Finally, it is necessary to correctly determine the H_{EB} values (see above) and the saturation magnetization of the FM subsystem (here, strong external fields are needed to reach the saturation of the contribution of the FM subsystem, which manifests itself as a field-linear portion of the $M(H)$ dependence [8, 10, 14, 15, 25]). The specific binding energy σ_S was estimated using Eq. (5) for CuO and NiO AFM nanoparticles in [31, 32], where the particle size D was used as d_{FM}.

The exchange coupling between the magnetic subsystems should also manifest itself in the FC remanent magnetization value. By analogy with Eq. (2), we can write the expression for the excess remanent magnetization M_{R_EB}

$$M_{R\_EB} = M_{R\_FC} - M_{R\_INF}. \qquad (6)$$

The M_{R_EB} value may depend on the binding energy σ_S in a fairly complex way; therefore, it is difficult to directly estimate σ_S from M_{R_EB}. Nevertheless, the exchange coupling can be reflected in the relaxation of the remanent magnetization, i.e., in the $M_{R\_FC}(t)$ dependence. Figure 4 shows the M_{R_FC} and M_{R_ZFC} values after relaxation for 4500 s. It can be seen that the $M_{R\_FC}(t = 4500$ s) value is significantly higher than M_{R_INF} and such a behavior is apparently characteristic of the systems with the exchange bias effect.

The relaxation of the remanent magnetization of single-domain magnetic particles is associated with the change in the projections of their magnetic moments onto the applied field direction. In this case, the magnetic moments must overcome the potential barriers caused by the magnetic anisotropy due to thermal fluctuations. The investigations of the probability of hoppings of the particle magnetic moments through potential barriers with height U [51] yield the frequently observed logarithmic time dependence of the magnetization

$$M(t) = M(t_0)(1 - (k_BT/U)\ln(t/t^*)). \qquad (7)$$

Here, $M(t_0)$ is the magnetization at the initial instant of time, k_B is the Boltzmann constant, and t^* is the constant. Logarithmic dependence (7) is usually observed at $t \ge 10^2$ s [51–53]. The height U of the potential barrier at $H = 0$ (after switching-off the field) should be determined by the height of the barriers that

occurred after switching-on the field. Consequently, the U value determined from the FC relaxation measurements at $H = 0$ should contain the contribution of the energy of exchange coupling between nanoparticle magnetic subsystems.

Figure 5 shows the normalized dependences of the remanent magnetization $M_{R\_FC}(t)/M_{R\_FC}(t = 0)$ and $M_{R\_ZFC}(t)/M_{R\_ZFC}(t = 0)$ obtained for the investigated sample. In this figure, the logarithmic scale is used along the abscissa axis. For the data obtained, logarithmic dependence (7) is valid starting with $t^* \sim 10^2$ s. The slopes of the FC and ZFC relaxation dependences are noticeably different. For the $M_{R\_FC}(t)$ dependence, the U value determined from Eq. (7) is 250 K, while under the ZFC conditions the barrier energy U is 95 K. This difference is indicative of a significant increase in the height of the energy barriers for the magnetic moments under the FC conditions and obviously reflects the exchange coupling between nanoparticle magnetic subsystems.

Let us estimate the specific binding energy of the magnetic subsystems using the standard approach (Eq. (5)) and through the barrier energies U calculated from the measured remanent magnetization relaxation. For simplicity, we assume, as in [31, 32], that $d_{FM} \approx D$ (at $D \approx 4$ nm). Then, at a value of $M_S \approx 20$ G typical of ferrihydrite [12, 13, 44] and $H_{EB} \approx 1.25$ kOe for sample FH-4 nm, we obtain, using Eq. (5), a value of $\sigma_S \approx 0.01$ erg/cm^2. If we compare the potential barrier U_{ZFC} for the ZFC mode with the potential barrier U_{FC} for the FC mode, their difference should be proportional to the energy E_{EB} of the exchange coupling of the magnetic subsystems

$$E_{EB} \sim U_{FC} - U_{ZFC}. \quad (8)$$

According to the analysis of the magnetization relaxation data, the value $U_{FC} - U_{ZFC}$ is ≈150 K. The U_{ZFC} value apparently slightly increases if the H_{max} value under the ZFC conditions is high (~10^5 Oe) and the M_{R_ZFC} value is close to M_{R_INF} (see Fig. 4). We set $(U_{FC} - U_{ZFC}) \sim 10^2$ K and the area S of the interface between the magnetic subsystems in the AFM nanoparticle to be equal to the particle surface area, i.e., $S \sim \pi D^2$. Then, using the obvious relation

$$\sigma_S = E_{EB}/S, \quad (9)$$

we obtain $\sigma_S \approx 0.027$ erg/cm^2. This value is larger than the value obtained using the standard approach by a factor of approximately 2.5 ($\sigma_S \approx 0.01$ erg/cm^2 from Eq. (5)). Thus, only qualitative agreement is observed, but both methods have the same drawback, specifically, the ambiguity of determination of the main parameters (the d_{FM} and S values). At the same time, the qualitative agreement between the estimated σ_S values suggests the possibility of using the remanent magnetization relaxation processes to calculate the energy of the exchange coupling between magnetic

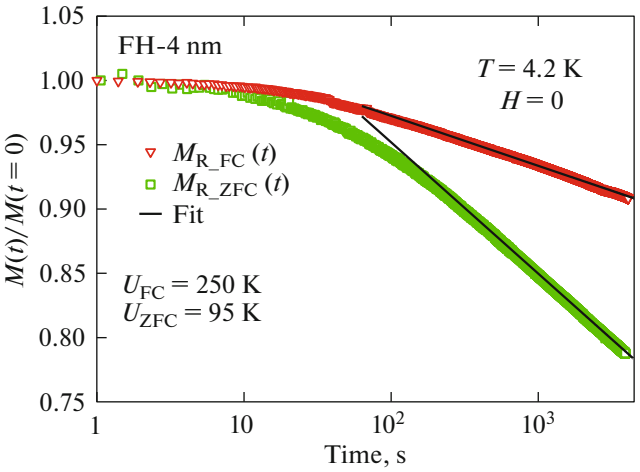

Fig. 5. Normalized time dependences of the remanent magnetization (logarithmic scale) under the FC ($M_{R\_FC}(t)/M_{R\_FC}(t = 0)$) and ZFC ($M_{R\_ZFC}(t)/M_{R\_ZFC}(t = 0)$) conditions (symbols). Solid lines are built using Eq. (7) basing on the condition of the best agreement with the experimental data at $t > 10^2$ s.

subsystems in AFM nanoparticles. It is worth noting that the obtained value σ_S (0.01–0.03 erg/cm^2) is similar to the specific energy of the exchange coupling of NiO nanoparticles (0.03 erg/cm^2) [31] and exceeds that for CuO nanoparticles (6×10^{-5} erg/cm^2) [32].

Thus, the use of the barrier energies determined from the remanent magnetization relaxation for establishing the exchange bias effect in AFM nanoparticles is an alternative to the conventional method in which only the exchange bias field is analyzed. In addition, note the possibility of analyzing the excess remanent magnetization M_{R_EB} (Eq. (6)). For AFM nanoparticles, this parameter is more important than for the FM/AFM structures. This statement is based on the similarity of the dependences of H_{EB} and M_{R_EB} on the ferrihydrite particle size D (Fig. 6). In the figure, the data obtained in [42, 43] on the biogenic and chemical ferrihydrite samples are summarized. It follows from the data in Fig. 6 that these curves are symbate, specifically, (i) the H_{EB} and M_{R_EB} growth with the particle size and (ii) the proportionality of the H_{EB} and M_{R_EB} values at the same particle size. It should be noted that the dependences of H_{EB} on the size D of NiO and CuO nanoparticles were obtained in [31, 32]. In these dependences, H_{EB} also increases to a certain D value and then decreases (for submicron AFM particles, no noticeable exchange bias effect is observed). The obtained information on the $H_{EB}(D)$ and $M_{R\_EB}(D)$ dependences, the interrelation between $H_{EB}(D)$ and $M_{R\_EB}(D)$, and the relaxation of $M_{R\_EB}(D)$ give faith to understanding the mechanisms of the exchange bias effect in AFM nanoparticles.

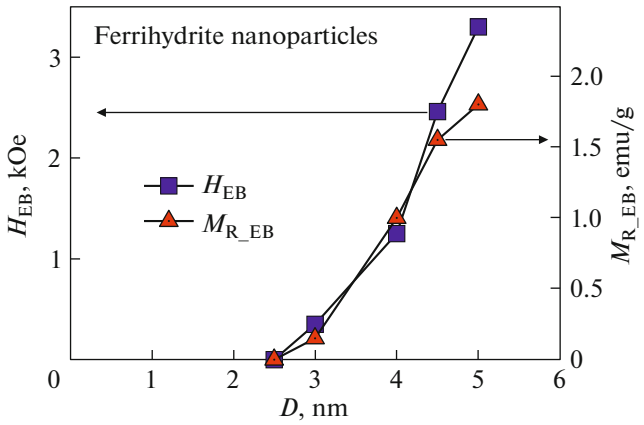

Fig. 6. Dependences of the exchange bias field H_{EB} and excess remanent magnetization M_{R_EB} (Eq. (6)) on the ferrihydrite particle size D according to the results reported in [42, 43]. The data for the sample investigated in this work correspond to $D = 4$ nm.

4. CONCLUSIONS

AFM nanoparticles exhibit the shift of the magnetic hysteresis loop upon cooling in an external field starting only with a certain particle size, which is ~3 nm for ferrihydrite. This effect is related to the presence of the exchange coupling between the magnetic subsystems formed in antiferromagnetically ordered nanoparticles. An important feature of such objects is that, here, the exchange bias effect leads to the shift of the magnetic hysteresis loop both along the abscissa and ordinate axis. This makes it possible to analyze the behavior of the remanent magnetization of AFM systems under exchange bias. For the samples of ferrihydrite nanoparticles with different average sizes, the excess remanent magnetization, i.e., the quantity similar to the exchange bias field H_{EB} behaves similarly to $H_{EB}(D)$ upon variation in the particle size D.

The study of relaxation of the remanent magnetization of ferrihydrite nanoparticles with an average size of 4 nm allowed us to establish the following. (i) The remanent magnetization noticeably decreases with time after cooling both in the field and without it. (ii) A relative decrease in the remanent magnetization is much larger under the zero field cooling conditions. (iii) The logarithmic time dependence of the remanent magnetization relaxation is observed starting with ~10^2 s. This allows us to interpret the relaxation data using commonly accepted Eq. (7) and to obtain the barrier energies in the presence of the exchange coupling (field cooling) and under standard conditions (zero field cooling). Therefore, we can estimate the energy of exchange coupling between the magnetic subsystems (Eq. (9)), which is of the same order of magnitude as the value obtained by a standard analysis of the exchange bias field (Eq. (5)).

Thus, in this study, we demonstrated by an example of ferrihydrite nanoparticles that the analysis of the remanent magnetization and its relaxation under the exchange bias makes it possible to estimate the energy of the exchange coupling between the magnetic subsystems formed in AFM nanoparticles. This method is an alternative to the standard approach, which only analyzes the exchange bias field determined from the shift of the $M(H)$ hysteresis loop along the field axis.

CONFLICT OF INTEREST

The authors declare that they have no conflicts of interest.

REFERENCES

1. L. Néel, C. R. Acad. Sci. (Paris) **252**, 4075 (1961).
2. S. Mørup, D. E. Madsen, C. Fradsen, C. R. H. Bahl, and M. F. Hansen, J. Phys.: Condens. Matter **19**, 213202 (2007).
3. Yu. L. Raikher and V. I. Stepanov, J. Exp. Theor. Phys. **107**, 435 (2008).
4. N. J. O. Silva, V. S. Amaral, and L. D. Carlos, Phys. Rev. B **71**, 184408 (2005).
5. M. S. Seehra and A. Punnoose, Phys. Rev. B **64**, 132410 (2001).
6. C. Rani and S. D. Tiwari, J. Magn. Magn. Mater. **385**, 272 (2015).
7. J. G. E. Harris, J. E. Grimaldi, D. D. Awschalom, A. Cholero, and D. Loss, Phys. Rev. B **60**, 3453 (1999).
8. C. Gilles, P. Bonville, H. Rakoto, J. M. Broto, K. K. W. Wong, and S. Mann, J. Magn. Magn. Mater. **241**, 430 (2002).
9. A. A. Lepeshev, I. V. Karpov, A. V. Ushakov, D. A. Balaev, A. A. Krasikov, A. A. Dubrovskiy, D. A. Velikanov, and M. I. Petrov, J. Supercond. Nov. Magn. **30**, 931 (2017).
10. D. A. Balaev, A. A. Dubrovskiy, A. A. Krasikov, S. I. Popkov, A. D. Balaev, K. A. Shaikhutdinov, V. L. Kirillov, and O. N. Mart'yanov, Phys. Solid State **59**, 1547 (2017).
11. D. A. Balaev, A. A. Dubrovskii, A. A. Krasikov, S. V. Stolyar, R. S. Iskhakov, V. P. Ladygina, and E. D. Khilazheva, JETP Lett. **98**, 139 (2013).
12. D. A. Balaev, A. A. Krasikov, A. A. Dubrovskii, S. V. Semenov, O. A. Bayukov, S. V. Stolyar, R. S. Iskhakov, V. P. Ladygina, and L. A. Ishchenko, J. Exp. Theor. Phys. **119**, 479 (2014).
13. D. A. Balaev, A. A. Krasikov, A. A. Dubrovskiy, S. I. Popkov, S. V. Stolyar, O. A. Bayukov, R. S. Iskhakov, V. P. Ladygina, and R. N. Yaroslavtsev, J. Magn. Magn. Mater. **410**, 71 (2016).
14. S. I. Popkov, A. A. Krasikov, D. A. Velikanov, V. L. Kirillov, O. N. Martyanov, and D. A. Balaev, J. Magn. Magn. Mater. **483**, 21 (2019).
15. S. I. Popkov, A. A. Krasikov, A. A. Dubrovskiy, M. N. Volochaev, V. L. Kirillov, O. N. Martyanov, and D. A. Balaev, J. Appl. Phys. **126**, 103904 (2019).
16. C. Diaz-Guerra, M. Vila, and J. Piqueras, Appl. Phys. Lett. **96**, 193105 (2010).

17. D. A. Balaev, A. A. Krasikov, D. A. Velikanov, S. I. Popkov, N. V. Dubynin, S. V. Stolyar, V. P. Ladygina, and R. N. Yaroslavtsev, Phys. Solid State **60**, 1973 (2018).
18. R. H. Kodama and A. E. Berkowitz, Phys. Rev. B **59**, 6321 (1999).
19. Yu. A. Koksharov, S. P. Gubin, I. D. Kosobudsky, G. Yu. Yurkov, D. A. Pankratov, L. A. Ponomarenko, M. G. Mikheev, M. Beltran, Y. Khodorkovsky, and A. M. Tishin, Phys. Rev. B **63**, 012407 (2000).
20. E. Winkler, R. D. Zysler, M. Vasquez Mansilla, and D. Fiorani, Phys. Rev. B **72**, 132409 (2005).
21. M. Tadic, D. Nikolic, M. Panjan, and G. R. Blake, J. Alloys Compd. **647**, 1061 (2015).
22. S. V. Stolyar, D. A. Balaev, V. P. Ladygina, A. I. Pankrats, R. N. Yaroslavtsev, D. A. Velikanov, and R. S. Iskhakov, JETP Lett. **111**, 183 (2020).
23. M. Tadić, M. Panjan, D. Marković, I. Milošević, and V. Spasojević, J. Alloys Compd. **509**, 7134 (2011).
24. A. S. Kamzin, A. A. Valiullin, V. G. Semenov, H. Das, and N. Wakiya, Phys. Solid State **61**, 1113 (2019).
25. N. J. O. Silva, A. Millan, F. Palacio, E. Kampert, U. Zeitler, and V. S. Amaral, Phys. Rev. B **79**, 104405 (2009).
26. W. P. Meiklejohn and C. P. Bean, Phys. Rev. **102**, 1413 (1956).
27. J. Nogués and I. K. Schuller, J. Magn. Magn. Mater. **192**, 203 (1999).
28. S. Giri, M. Patra, and S. Majumdar, J. Phys.: Condens. Matter **23**, 073201 (2011).
29. J. Noguées, J. Sort, V. Langlais, V. Skumryev, S. Suriñach, J. S. Muñoz, and M. D. Baró, Phys. Rep. **422**, 65 (2005).
30. S. A. Makhlouf, F. T. Parker, F. E. Spada, and A. E. Berkowitz, J. Appl. Phys. **81**, 5561 (1997).
31. S. A. Makhlouf, H. Al-Attar, and R. H. Kodama, Solid State Commun. **145**, 1 (2008).
32. M. S. Seehra and A. Punnoose, Solid State Commun. **128**, 299 (2003).
33. A. Punnoose and M. S. Seehra, J. Appl. Phys. **91**, 7766 (2002).
34. A. Punnoose, H. Magnone, M. S. Seehra, and J. Bonevich, Phys. Rev. B **64**, 174420 (2001).
35. A. E. Bianchi, S. J. Stewart, R. D. Zysler, and G. Punte, J. Appl. Phys. **112**, 083904 (2012).
36. S. A. Makhlouf, F. T. Parker, and A. E. Berkowitz, Phys. Rev. B **55**, R14717 (1997).
37. A. Punnoose, T. Phanthavady, M. S. Seehra, N. Shah, and G. P. Huffman, Phys. Rev. B **69**, 054425 (2004).
38. T. S. Berquó, J. J. Erbs, A. Lindquist, R. L. Penn, and S. K. Banerjee, J. Phys.: Condens. Matter **21**, 176005 (2009).
39. M. S. Seehra, V. Singh, X. Song, S. Bali, and E. M. Eyring, J. Phys. Chem. Solids **71**, 1362 (2010).
40. D. A. Balaev, A. A. Krasikov, A. A. Dubrovskii, S. V. Semenov, S. I. Popkov, S. V. Stolyar, R. S. Iskhakov, V. P. Ladygina, and R. N. Yaroslavtsev, Phys. Solid State **58**, 287 (2016).
41. N. J. O. Silva, V. S. Amaral, A. Urtizberea, R. Bustamante, A. Millán, F. Palacio, E. Kampert, U. Zeitler, S. de Brion, O. Iglesias, and A. Labarta, Phys. Rev. B **84**, 104427 (2011).
42. D. A. Balaev, A. A. Krasikov, A. A. Dubrovskiy, S. I. Popkov, S. V. Stolyar, R. S. Iskhakov, V. P. Ladygina, and R. N. Yaroslavtsev, J. Appl. Phys. **120**, 183903 (2016).
43. S. V. Stolyar, D. A. Balaev, V. P. Ladygina, A. A. Dubrovskiy, A. A. Krasikov, S. I. Popkov, O. A. Bayukov, Yu. V. Knyazev, R. N. Yaroslavtsev, M. N. Volochaev, R. S. Iskhakov, K. G. Dobretsov, E. V. Morozov, O. V. Falaleev, E. V. Inzhevatkin, O. A. Kolenchukova, and I. A. Chizhova, J. Supercond. Nov. Magn. **31**, 2297 (2018).
44. S. V. Stolyar, R. N. Yaroslavtsev, R. S. Iskhakov, O. A. Bayukov, D. A. Balaev, A. A. Dubrovskii, A. A. Krasikov, V. P. Ladygina, A. M. Vorotynov, and M. N. Volochaev, Phys. Solid State **59**, 555 (2017).
45. Yu. L. Raikher, V. I. Stepanov, S. V. Stolyar, V. P. Ladygina, D. A. Balaev, L. A. Ishchenko, and M. Balashoyu, Phys. Solid State **52**, 298 (2010).
46. S. V. Stolyar, O. A. Bayukov, V. P. Ladygina, R. S. Iskhakov, L. A. Ishchenko, V. Yu. Yakovchuk, K. G. Dobretsov, A. I. Pozdnyakov, and O. E. Piksina, Phys. Solid State **53**, 100 (2011).
47. L. Anghel, M. Balasoiu, L. A. Ishchenko, S. V. Stolyar, T. S. Kurkin, A. V. Rogachev, A. I. Kuklin, Y. S. Kovalev, Y. L. Raikher, R. S. Iskhakov, and G. Duca, J. Phys.: Conf. Ser. **351**, 12005 (2012).
48. D. A. Balaev, A. A. Krasikov, S. V. Stolyar, R. S. Iskhakov, V. P. Ladygina, R. N. Yaroslavtsev, O. A. Bayukov, A. M. Vorotynov, M. N. Volochaev, and A. A. Dubrovskii, Phys. Solid State **58**, 1782 (2016).
49. A. D. Balaev, Yu. V. Boyarshinov, M. M. Karpenko, and B. P. Khrustalev, Prib. Tekh. Eksp., No. 3, 167 (1985).
50. A. P. Malozemoff, J. Appl. Phys. **63**, 3874 (1988).
51. J. Tejada, X. X. Zhang, and E. M. Chudnovsky, Phys. Rev. B **47**, 14977 (1993).
52. R. Prozorov, Y. Yeshurun, T. Prozorov, and A. Gedanken, Phys. Rev. B **59**, 6956 (1999).
53. J. Tejada and X. X. Zhang, J. Phys.: Condens. Matter **6**, 263 (1994).

Translated by E. Bondareva